Self-Responsive Biomimetic Short Lipopeptide-Based Delivery Systems for Enhanced Antibiotic Efficacy against Drug-Resistant Infections

Shruti Sharma[a], Deepanshi Saxena [b], Aanand Kautu[a], Sidharth Chopra*[b], Khashti Ballabh Joshi*[a]

[a.]Department of Chemistry, School of Chemical Science and Technology, Dr. Harisingh Gour Vishwavidyalaya (A Central University), Sagar- 470003, Madhya Pradesh India.
Email: kbjoshi77@gmail.com; kbjoshi@dhsgsu.edu.in.

[b.]Department of Microbiology, CSIR-Central Drug Research Institute, Sitapur Road, Janakipuram Extension, Lucknow, India, E-mail: skchopra007@gmail.com

Supplementary Information

1.0 Materials and Methods (General)- The solvents and reagents used in this study were sourced from various commercial suppliers according to specific requirements L-Tyrosine was obtained from Spectrochem, Mumbai, India. The palmitic acid linker was sourced from SRL Pvt. Ltd., India. Peptide coupling agents, including N,N´-dicyclohexylcarbodiimide (DCC), N-hydroxybenzotriazole (HOBt), and 1-ethyl-3-(3-dimethylaminopropyl) carbodiimide (EDC·HCl), were supplied by Avra Synthesis Pvt. Ltd., Hyderabad, India. The protecting agent, Di-tert-butyl dicarbonate (Boc anhydride), and the deprotecting agent, Trifluoroacetic acid (TFA), were also sourced from Spectrochem Pvt. Ltd. Organic bases such as triethylamine (Et_3N), diisopropylethylamine (DIPEA), and 4-Dimethylaminopyridine (DMAP) were provided by S D Fine-Chem Ltd. Strong anion exchange resin (Dowex 1-X8) was obtained from HiMedia Laboratories Pvt. Ltd., India, while strong cation exchange resin (Amberlite IR-120 Na form) was purchased from Spectrochem Pvt. Ltd., Mumbai, India. Silica gel with mesh sizes of 60-120 and 100-200, as well as pre-coated aluminum sheets for thin-layer chromatography (TLC Silica gel 60 F254), were procured from Merck Chemicals, India. Solvents such as methanol (MeOH), ethanol (EtOH), dichloromethane (DCM), ethyl acetate (EtOAc), acetone (Ac_2O), chloroform ($CHCl_3$), dimethylsulfoxide (DMSO), diethyl ether (Et_2O), acetonitrile (ACN), pyridine, N, N-dimethylformamide (DMF), and tetrahydrofuran (THF) were purchased from S D Fine Chemicals Ltd., India. Additionally, HPLC-grade solvents and deuterated solvents for recording nuclear magnetic resonance (NMR) spectra were acquired from Merck Pvt. Ltd.

2.0 Peptide Synthesis- The tripeptide Tyr-Tyr-β-Ala was synthesized using conventional solution-phase techniques, following a well-established protocol developed by our research group, as detailed in our previous publications.[1,2] Subsequently, the tripeptide was conjugated with palmitic acid to produce short peptide amphiphiles(sPA).[3,4] The purity and identity of these synthesized compounds were rigorously confirmed prior to their use in further experiments. All synthetic procedures were carried out under ambient room temperature conditions.

3.0 UV-Vis studies- A 10 μM solution of sPA in ethanol was prepared from stock solution of 500 μM. Additionally, a 1 mM stock solution of meropenem was prepared in sterile water and prepared it upto 500 μM . A solution of 10 μM peptide (sPA) was titrated with the meropenem stock solution, incrementally increasing the concentration of meropenem 0 μM up to 20 μM. UV-Vis absorption spectra were recorded at each titration step.[5] All spectral measurements were performed using a LABINDIA UV 3092 spectrophotometer with a 10 mm quartz cuvette, and the temperature was precisely controlled at 25±0.1 °C throughout the experiment.

4.0 Transmission Electron Microscopy (TEM)- Freshly prepared 2 μL aliquots of every test sample (sPA) were transferred to 400 mesh carbon-coated copper grids and dried at room temperature for overnight, followed by vacuum drying. The samples were analyzed with the FEI Technai 20 U Twin Transmission Electron Microscope.[6]

5.0 Fluorescence Optical Microscopy- Self-assembled structures of sPA and sPA formulated MEPM samples were examined under a fluorescent optical microscope (LABINDIA Nikon Eclipse C*i*-E) in a dark field in addition to bright field under 100x. 1mM of the test samples solutions were incubated for 0-6 h with Rhodamine-B dye in ethanol/aqueous ethanol. The samples were mounted on glass slides and allowed to dry under Petri dish in a dust-free place. The dried samples were rinsed with distilled water 3×10s each for removal of excess and unbounded dye. The samples were dried and analysed under fluorescent optical microscope using red filter.[8,9]

6.0 FT-IR Study- Fourier-transform infrared (FT-IR) spectra were acquired using a Bruker Alpha II spectrometer equipped with an attenuated total reflectance (ATR) accessory. The FT-IR analysis was conducted to investigate the functional groups and secondary structural features of synthesized polyamides (sPA) and their complexes with meropenem (sPA-MEPM). Spectral data were collected over a wavenumber range of 4000–500 cm^{-1} with a spectral resolution of 4 cm^{-1}, utilizing a sample gain of 2 and averaging 32 scans for both sample and background to enhance signal quality. Data acquisition and processing, including noise reduction, were performed using OPUS 7.0 software.

For sample preparation, a 5 μL aliquot of a 50 μM solution of sPA and MEPM was applied onto a ZnSe crystal plate and subsequently air-dried.

7.0 Zeta Potential - The zeta potential of self-assembled sPA was determined by measuring its electrophoretic mobility using a laser-based multiple-angle particle electrophoresis analyzer (Malvern Zetasizer, DTS Ver. 4.10, Malvern Instruments, UK) and processed by NanoPlus software. The sPA nanostructures were dispersed in an aqueous medium and placed in an electrophoretic cell under an applied electric field of 15.24 V/cm, and the corresponding zeta potential was recorded.

8.0 Circular Dichroism spectroscopy- Circular dichroism (CD) spectra were recorded between 195 nm and 270 nm, with each spectrum representing the average of 3-5 scans. All measurements were conducted at 25 ± 0.1 °C. Spectra were collected for sPA and sPA-MEPM conjugates at a final concentration of 100 µM using a JASCO J-815 CD spectrometer with a 1-mm quartz cuvette. To account for baseline drift, background measurements of water or ethanol-water were subtracted from each sample.

9.0 Fluorescence study- Fluorescence spectra of test samples in the presence and absence of MEPM were recorded using a RF-5301PC Spectrofluorophotometer (Shimadzu) at room temperature with a 10-mm quartz cell. Samples were excited at λ_{ex} = 260 nm, and fluorescence intensity at 350 nm was measured to assess metal ion concentration dependence. HPLC-grade solvents were used. The interaction of MEPM with sPA was studied to understand its effect on fluorescence intensity and morphology.

Figures:

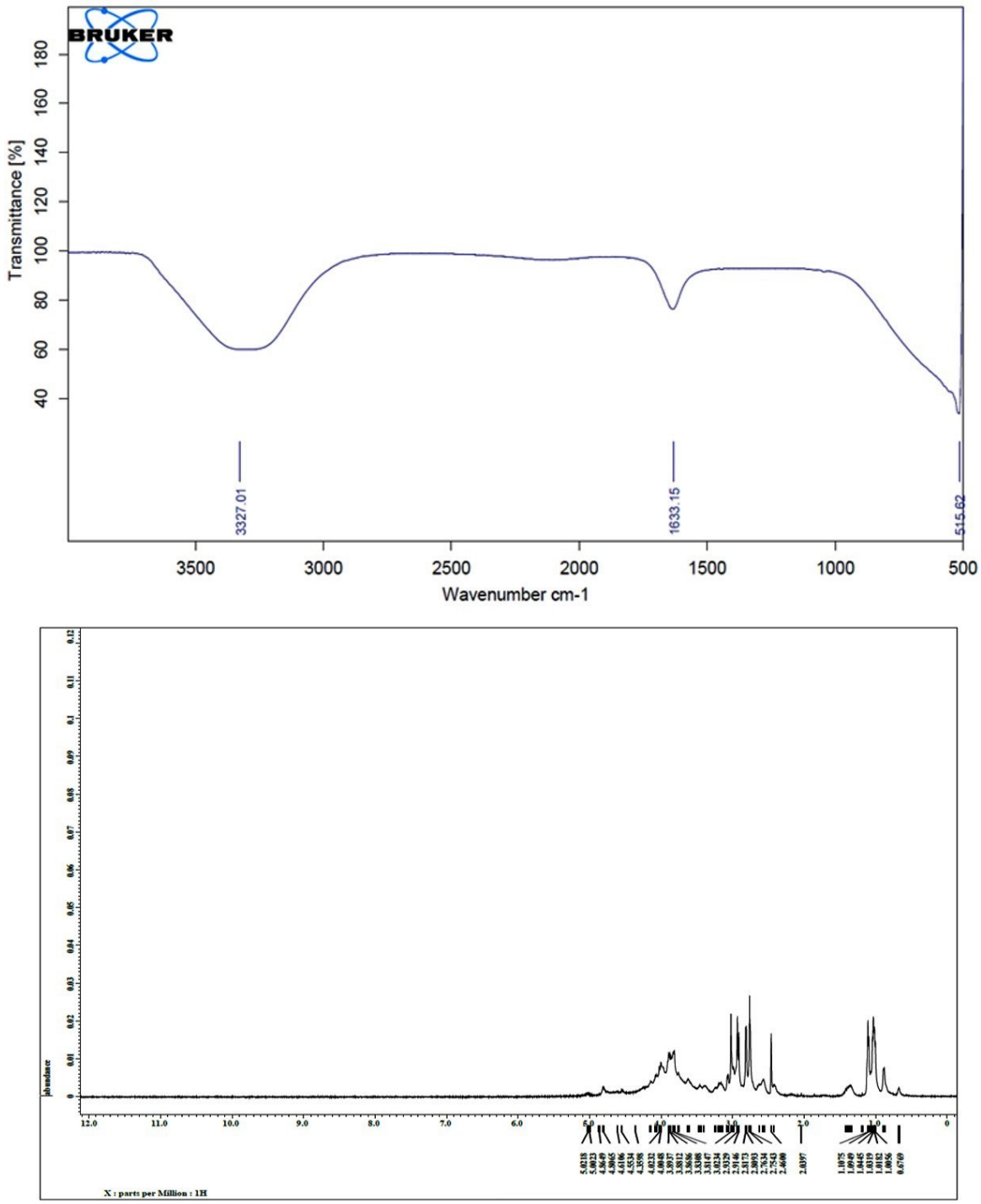

Figure S1: FT-IR (Top) and and 500-MHz ^{1}H-NMR(Bottom) of MEPM injection in DMSO-d_6.

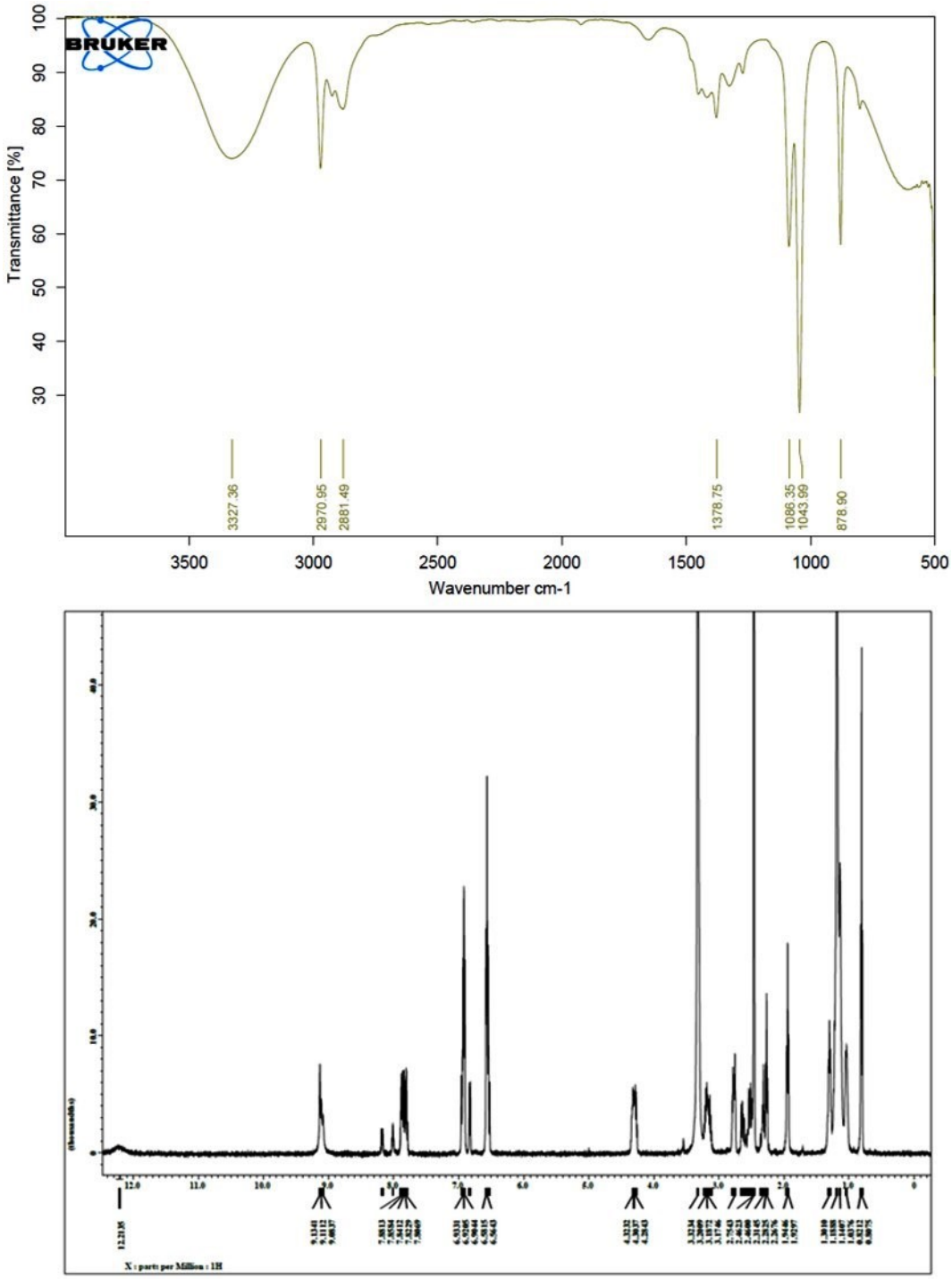

Figure S2: FT-IR (*top*) and 500-MHz ^{1}H-NMR(*bottom*) of sPA (Lipopeptide) alone in DMSO-d_6.

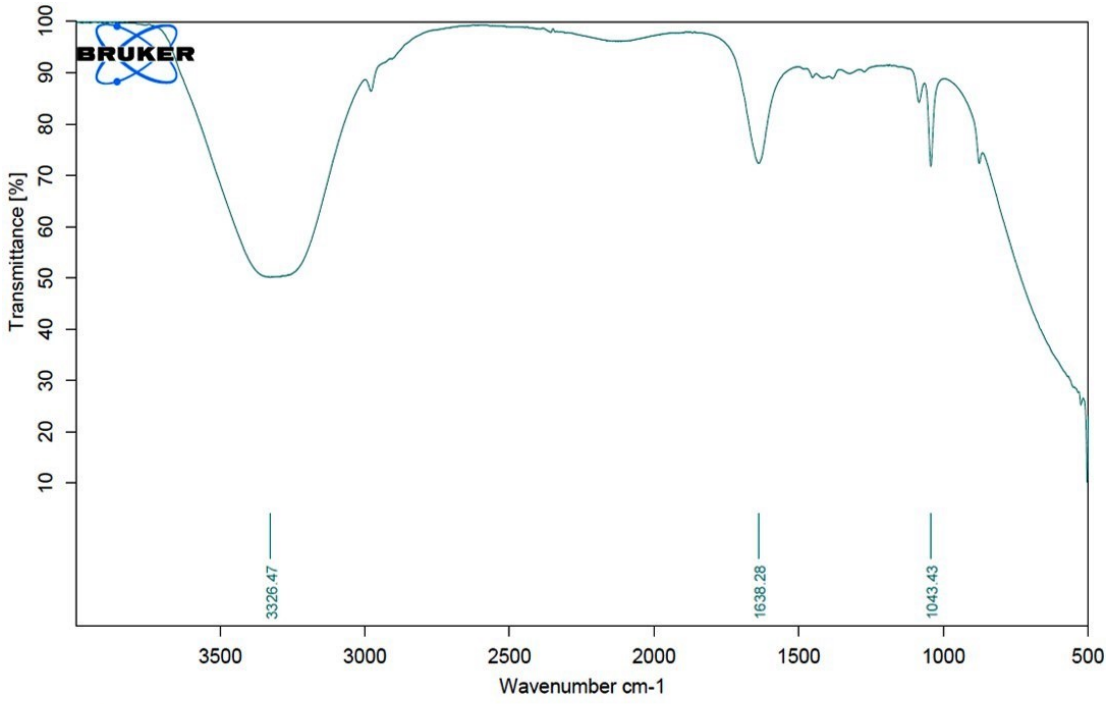

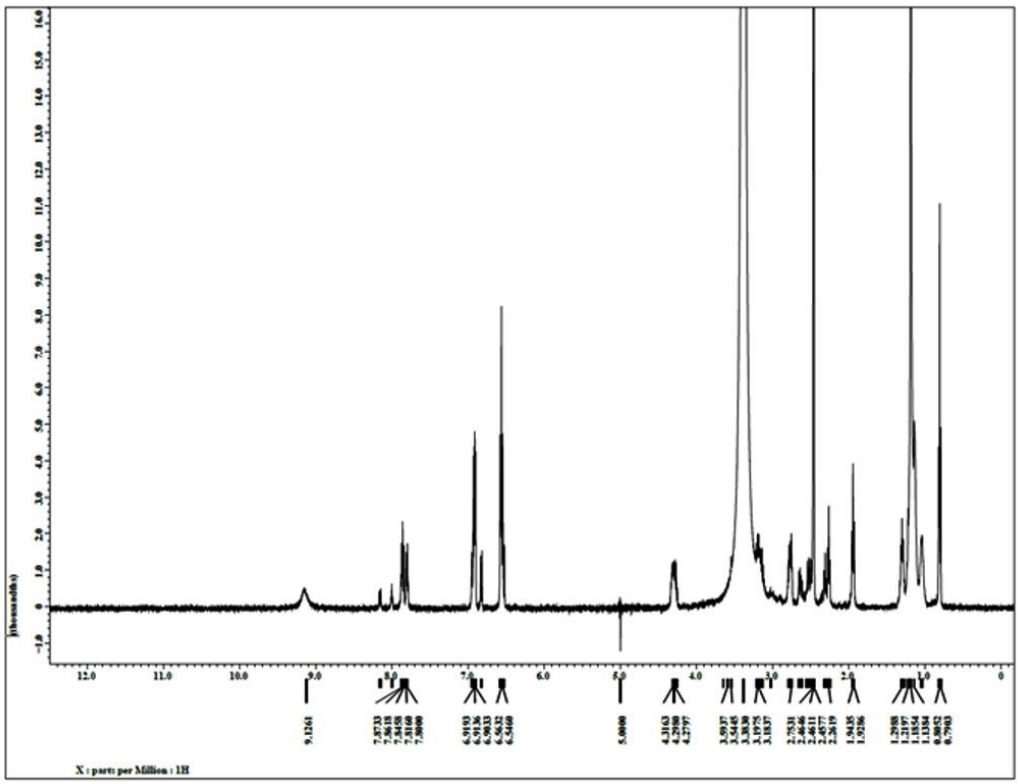

Figure S3: FT-IR (*top*) and 500-MHz ^{1}H-NMR(*bottom*) of sPA(Lipopeptide) with 0.2 equivalent MEPM in DMSO-d_6.

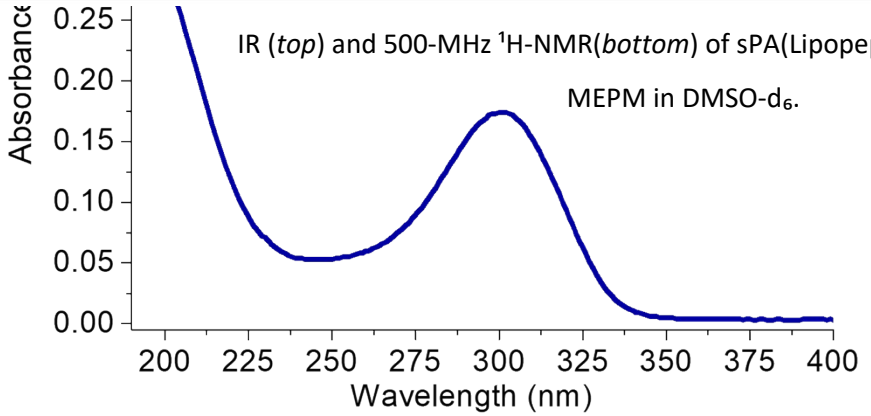

Figure S4. The picture depicts a UV-Visible graph of MEPM alone showing absorbance at 300 nm.

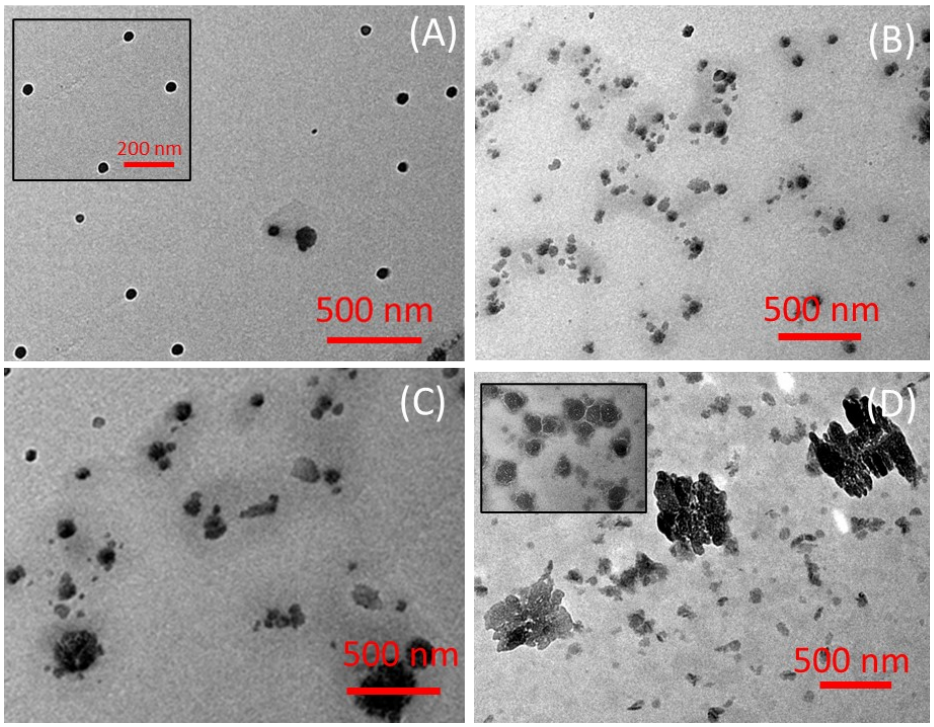

Figure S5. Time-dependent incubation studies of MEPM reveal the progressive evolution of nanostructures, likely attributable to MEPM degradation. (A) Freshly prepared MEPM displays uniform, spherical aggregate-like structures. (B) After 6 hours of incubation, the nanostructures undergo notable morphological changes, possibly due to the instability of MEPM under physiological conditions, as illustrated by the magnified image (C). (D) After 12 hours, morphological observations indicate complete degradation, initiating a transition in self-assembly from spherical to random aggregate formations.

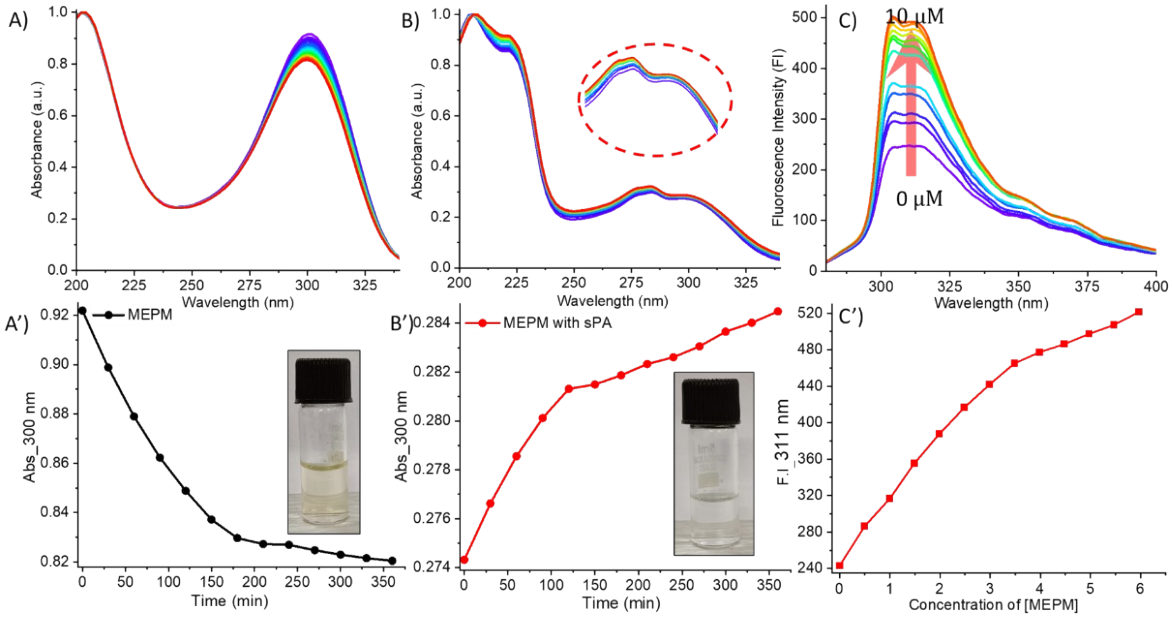

Figure S6: Stability profile (A, A'-B, B') of meropenem over time as confirmed by UV-Vis spectroscopy and colourimetry (inset). These findings are further substantiated by fluorescence spectroscopy (C-C'), where sPA was titrated with a MEPM sample (10^{-6} M). Notably, the fluorescence intensity at 311 nm, attributed to the tyrosine group, showed a marked increase, confirming the formation of a MEPM-sPA complex (λ_{ex} =260 nm, and λ_{em} = 310 nm). This complex formation provides aggregation-induced fluorescence enhancement, further supporting the stability and interaction between sPA and MEPM.

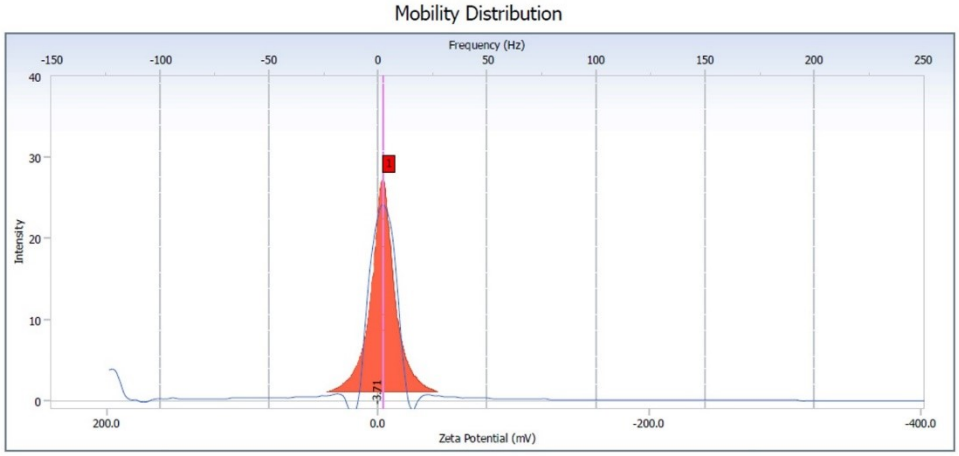

Measurement Results

Zeta Potential	: -3.71	(mV)	Doppler shift	: 2.31	(Hz)
Mobility	: -2.897e-005	(cm²/Vs)	Base Frequency	: 122.6	(Hz)
Conductivity	: 0.0437	(mS/cm)	Conversion Equation	: Smoluchowski	

Zeta Potential of Cell			Diluent Properties		
Upper Surface	: 20.60	(mV)	Diluent Name	: WATER	
Lower Surface	: -22.89	(mV)	Temperature	: 25.0	(°C)
Cell Condition			Refractive Index	: 1.3328	
Cell Type	: Flow Cell		Viscosity	: 0.8878	(cP)
Avg. Electric Field	: -16.65	(V/cm)	Dielectric Constant	: 78.3	
Avg. Current	: -0.03	(mA)			

Figure S7: The surface charge of sPA was calculated by zeta potential is -3.71 at physiological pH.

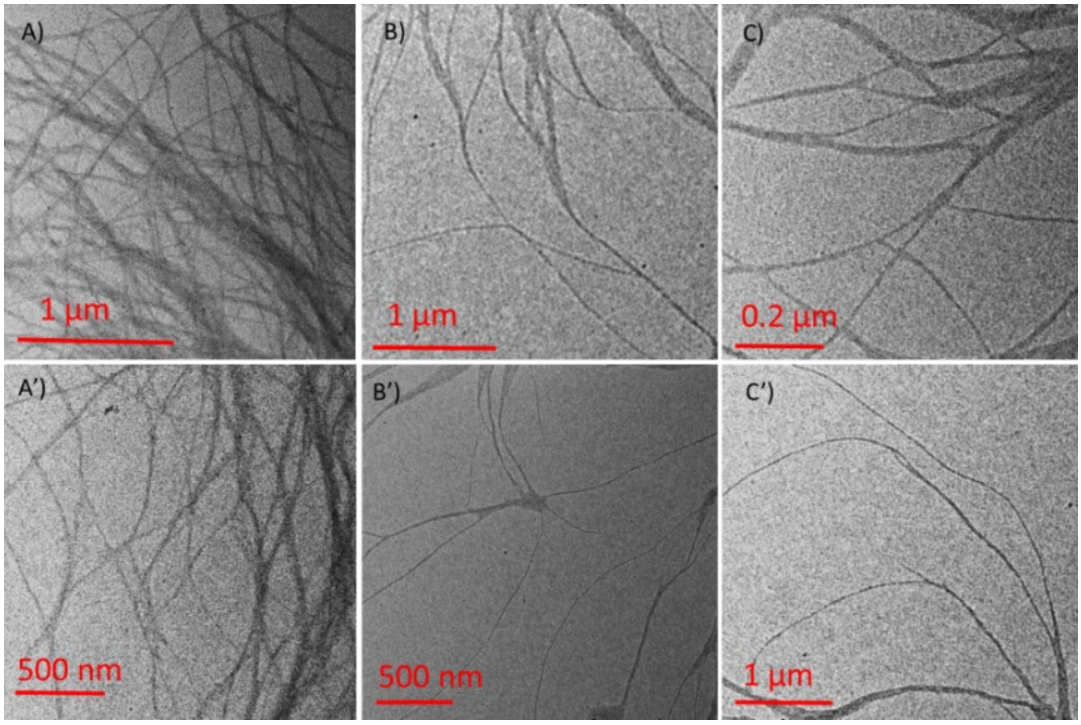

Figure S8. Additional supporting TEM images depict the self-assembled nanostructures of freshly prepared aqueous ethanolic sPA solution, revealing the formation of long, thin fibrous morphologies.

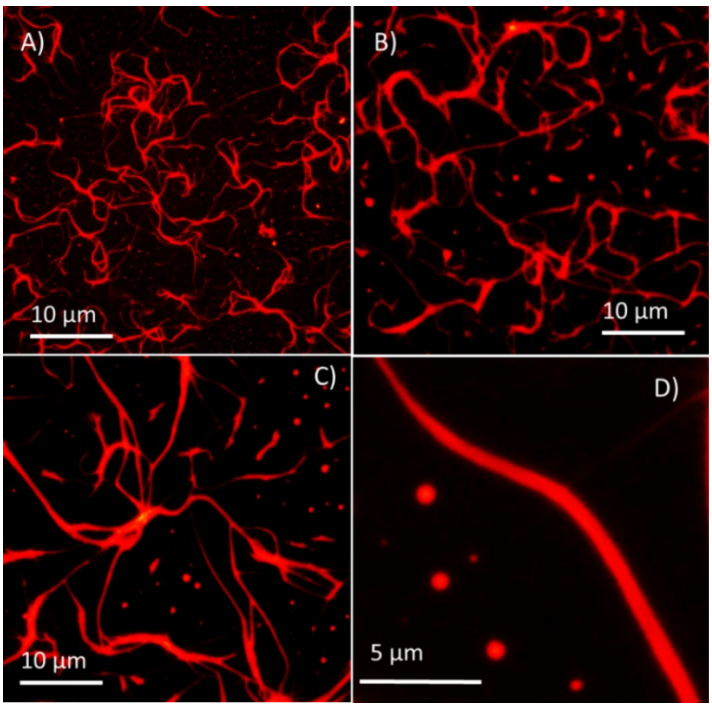

Figure S9. Fluorescence optical microscopy image of rhodamine B-stained self-assembled sPA nanostructures, displaying thin, straight fibers at a scale of 50 µm. This morphology suggests the potential of these sPA nanostructures for encapsulating chemical payloads.

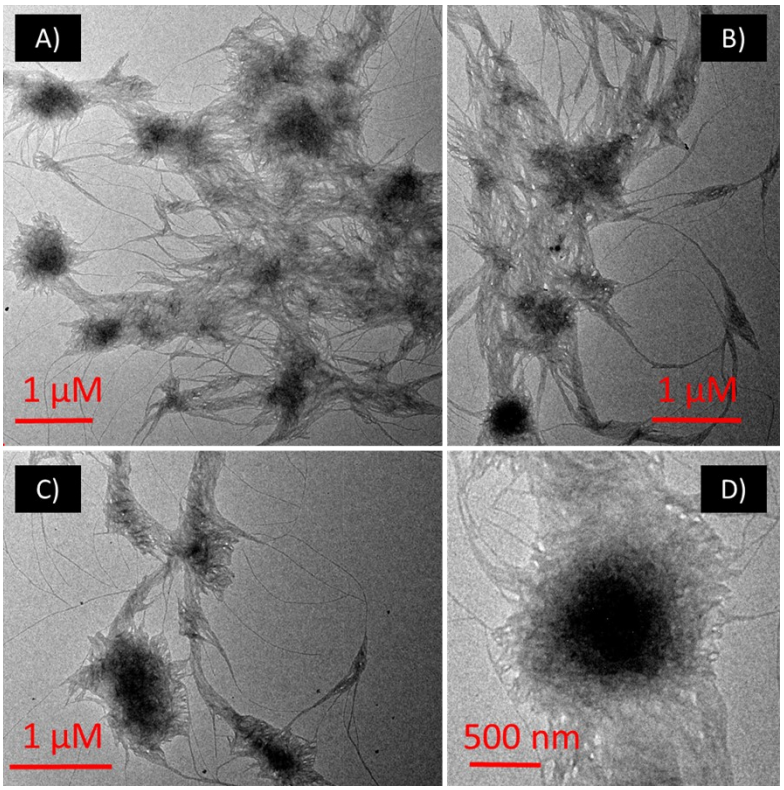

Figure S10. Additional TEM images reveal the morphological characteristics of sPA-MEPM nanostructures, showing the formation of nucleated and outwardly growing fibrous perhaps induced by the presence of MEPM.

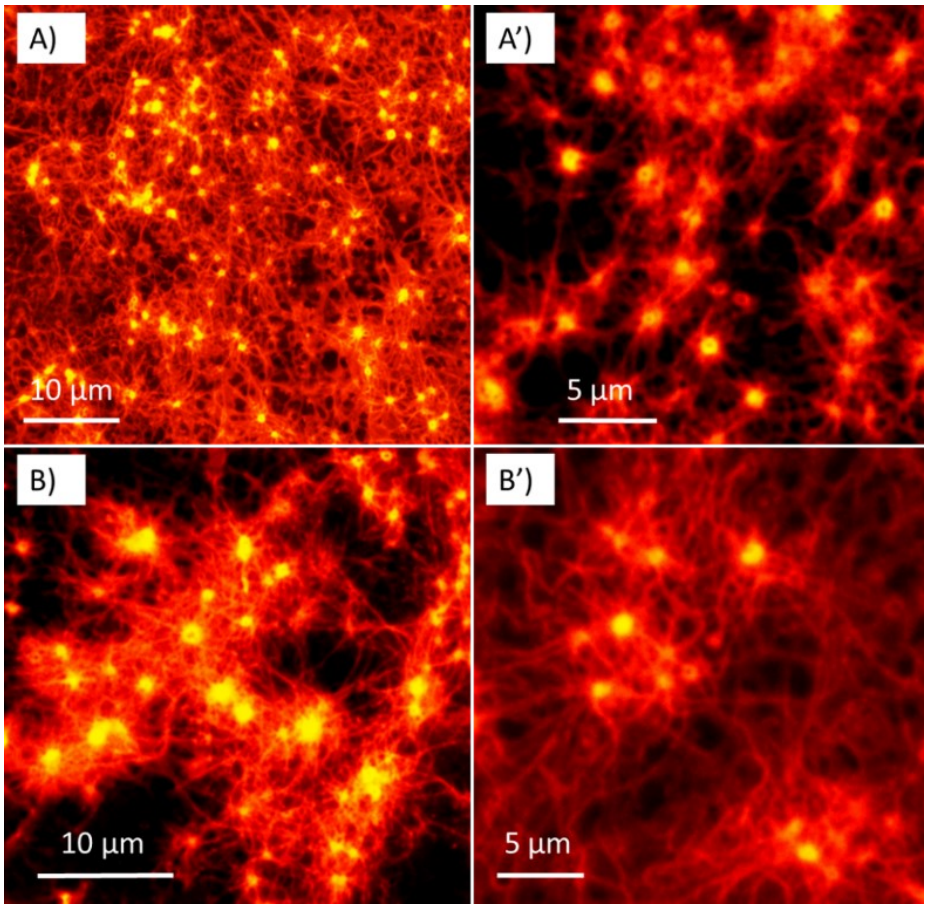

Figure S11. Rhodamine B-stained images illustrate the self-assembled structures of sPA-formulated MEPM samples, exhibiting a notable morphological shift from long, thin fibers to coagulated fibers at low resolution. This transition suggests interactions that promote the formation of nucleated, radially outward-growing fibrous assemblies, as evidenced by the altered fiber morphology.

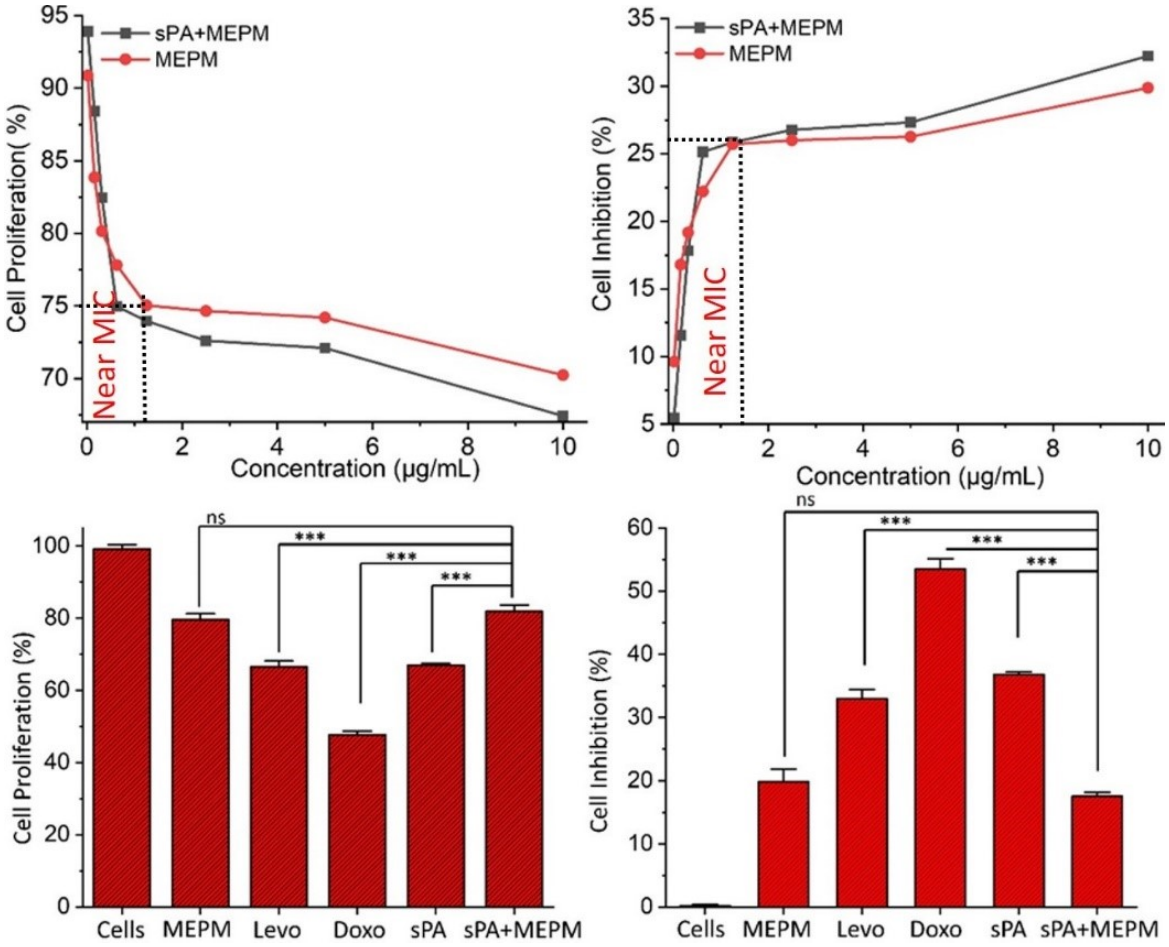

Figure S12. Cell proliferation and inhibition assays on healthy eukaryotic cells reveal significantly reduced cytotoxicity of sPA samples compared to standard therapeutics, including Doxorubicin, Levofloxacin, and Meropenem. Panels (A) and (B) show dose-dependent response curves, indicating that sPA-MEPM formulations exhibit notably lower toxicity near the MIC compared to Meropenem alone, highlighting an improved safety profile. Comparative analyses in Panels (C) and (D) reinforce the lower cytotoxicity of sPA and sPA-MEPM versus conventional drugs, supporting their potential as safer therapeutic alternatives. Statistical significance was assessed by one-way ANOVA, where *** ($p < 0.001$) indicates high significance, and ns ($p \geq 0.05$) indicates no significance.

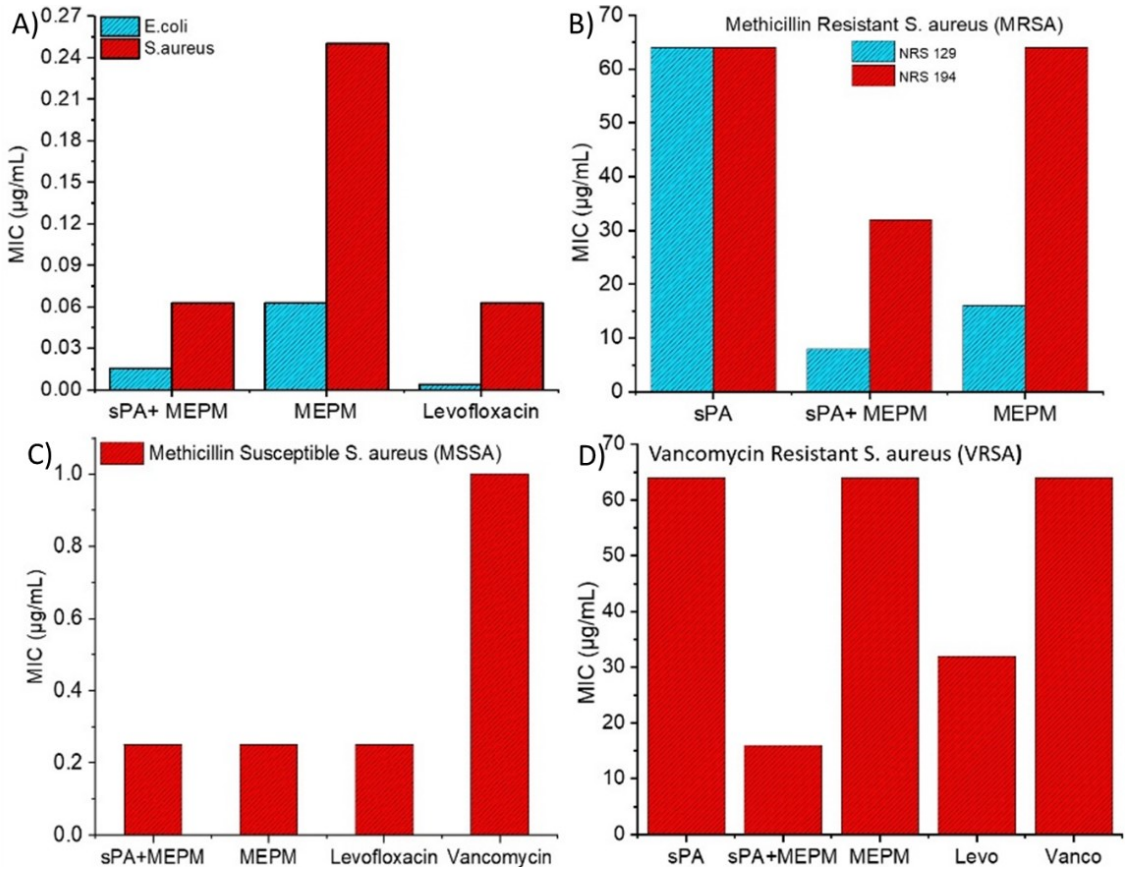

Figure S13. This figure presents the minimum inhibitory concentration (MIC) of various standard drugs, including nanoformulated sPA-MEPM, against multiple bacterial strains. Panel (A) compares the MIC of sPA-MEPM with Levofloxacin and Meropenem against *Escherichia coli* ATCC 25922 and *Staphylococcus aureus* ATCC 29213, demonstrating that sPA-MEPM achieves significant bacterial inhibition at lower concentrations. Panel (B) shows the MIC for methicillin-resistant *Staphylococcus aureus* (MRSA), where sPA-MEPM significantly reduces the MIC, indicating its efficacy against antibiotic-resistant strains. Panel (C) displays the MIC for methicillin-susceptible *Staphylococcus aureus* (MSSA), highlighting sPA-MEPM's superior bactericidal activity. Panel (D) depicts the MIC for vancomycin-resistant *Staphylococcus aureus* (VRSA), revealing a marked reduction in effective concentration with sPA-MEPM compared to standard drugs. These results underscore the potential of sPA-MEPM nanohybrids as an advanced antimicrobial therapy against multidrug-resistant bacterial infections.

References :

1. R. Singh, N. K. Mishra, V. Kumar, V. Vinayak, K. B. Joshi, *ChemBioChem.* 2018, **19**(15), 1630-1637.
2. R. Singh, N. K. Mishra, P. Gupta, K. B. Joshi, *Chem. Asian J.* 2020, **15**, 531 – 539.
3. K. Kesharwani, R. Singh, M. J. Khan, V. Vinayak, K. B. Joshi, *ChemistrySelect*. 2021, **6**, 6827-6833.
4. K. Kesharwani, A. Kautu, S. Sharma, R. Singh, V. Kumar, S. K. Tripathi, P. Shukla, K. B. Joshi, *Chem. Commun.* 2022, **58**, 13815-13818.

5. R. Singh, N. K. Mishra, N. Singh, P. Rawal, P. Gupta K. B. Joshi, *New J. Chem*. 2020, **44**, 9255.
6. S. K. Tripathi, K. Kesharwani, D. Saxena, R. Singh, A. Kautu, S. Sharma, A. Pandey, S. Chopra, K. B. Joshi, *ChemMedChem*. 2023, e202200654.
7. S. Sharma, A. Kautu, N. Singh, N. Kumar, V. Kumar, R. Singh, K. Kesharwani, N. Swain, P. Gupta, K. B. Joshi, *Next Materials.* 2024, **4**, 10118.
8. A. Kautu, S. Sharma, R. Singh, S. S Negi, N. Singh, N. Swain, N.; V. K. Namadeo, N. Kumar, P. Gupta, D. D. Bhatia, K. B. Joshi, *Nanoscale*. 2024, **16**, 14940-14952.
9. S. Sharma, A. Kautu, N. Kumar, N. Swain, V. Kumar, R. Singh, K. Kesharwani, N. Singh, P. Gupta K. B. Joshi, *Chemnanomat*. e202400098.
10. N. Swain, S. Sharma, R. Maitra, D. Saxena, A. Kautu, R. Singh, K. Kesharwani, S. Chopra, K. B. Joshi, *ChemMedChem.* 2024, **19**(8), e202300576.
11. K. Kesharwani, G. Kaul, A. Akhir, D. Saxena, R. Singh, N. K. Mishra, A. Pandey, S. Chopra, K. B. Joshi, *ChemMedChem*. 2022, **17**, e202200251.
12. N. Singh, R. Singh, M. Shukla, G. Kaul, S. Chopra, K. B. Joshi, S. Verma, *ACS Infect. Dis.* 2020, **6**, 2441−2450.
13. N. Singh, S. Sharma, R. Singh, S. Rajput, N. Chattopadhyay, D. Tewari, K. B. Joshi, S. Verma, *Chem. Sci.* 2021, **12**, 16085–16091.
14. A. Panjla, G. Kaul, M. Shukla, A. Akhir, S. Tripathi, A. Arora, S. Chopra, S. Verma, 2024, **176**, 116810.
15. R. Singh, S. Sharma, A. Kautu, K. B. Joshi, *Chem. Commun.* 2024, **60**, 7687-7696.